

# Super-resolution based generative adversarial network using visual perceptual loss function

Xuan Zhu<sup>1</sup>, Yue Cheng<sup>1</sup>, Rongzhi Wang<sup>1</sup>

<sup>1</sup>School of Information Science and Technology of Northwest University, Xi'an, People's Republic of China

Corresponding author: Xuan Zhu (e-mail: xuan\_zhu@126.com).

**Abstract:** In recent years, perceptual-quality driven super-resolution methods show satisfactory results. However, super-resolved images have uncertain texture details and unpleasant artifact. We build a novel perceptual loss function composed of morphological components adversarial loss and color adversarial loss and salient content loss to ameliorate these problems. The adversarial loss is applied to constrain color and morphological components distribution of super-resolved images and the salient content loss highlights the perceptual similarity of feature-rich regions. Experiments show that proposed method achieves significant improvements in terms of perceptual index and visual quality compared with the state-of-the-art methods.

## 1. Introduction

Single image super-resolution (SISR), which refers to recover a high-resolution (HR) image from a low-resolution (LR) image, is an ill-posed inverse problem. Many areas have an urgent and extensive requirement for SR, such as computer vision, medical image processing, and remote sensing image processing [1, 2]. Numerous SR methods such as interpolation-based methods [3, 4] and the learning-based methods [5, 6, 7] have been proposed. The interpolation methods use smooth and continuity assumptions of image to estimate the missing pixel values of the HR image, leading to jagged artifacts and blurring. The learning methods exploit the relationship between the LR image patch and the HR image patch to restore high-frequency details.

Recently, convolutional neural networks (CNNs) have made remarkable improvements in object recognition[8], object detection, semantic segmentation, super-resolution and neural style transfer, etc. For super-resolution, Dong et al. [9] first applied a lightweight convolutional neural network to super-resolve an LR image. It demonstrated excellent reconstruction quality compared with state-of-the-art methods at that time. Subsequently, considerable researches based on CNNs had been conducted for super-resolution. Kim et al [10] exploited recursive learning which relied on parameters sharing to improve performance without increasing computational burden. The deeper networks [12, 13, 14, 15] were constructed using residual learning proposed in [11] for more high-frequency details recovery. Tong et al [16] combined the low-level and high-level features of images using dense skip connections to boost the reconstruction performance significantly. These methods applied power signal-to-noise ratio (PSNR) value to evaluate the model performance and agree that higher PSNR value denotes better SR image quality and smaller distortion. However, the studies [18, 19, 20, 21] have shown the disagreement between common evaluation metrics (e.g. PSNR) and subjective evaluation of human observers. For example, [17] reported the highest PSNR value on benchmark dataset while blurry edge and poor visual quality were shown in their SR image. The study [32] claimed that there are two research directions, which are distortion-driven SR and perceptual-quality driven SR. The first minimize mean squared error (MSE) or absolute error between generated SR images and the target HR images to optimize super-resolution network, which favors a high PSNR. However, it shows over-smooth texture due to pixel-wise average of possible solutions. The second focuses on producing visually satisfactory

SR images. Various loss functions highly correlated with image visual features are applied to measure the reconstruction error between images. It recovers finer texture details but shows poor PSNR value. Most of the research work had been done around this direction. Dosovitskiy et al. [19] applied the content loss which minimizing MSE in the feature space instead of pixel space to ensure perceptual similarity between images. Cheon et al. [31] employed differential content loss to improve the reconstruction performance particularly for high-frequency components. The adversarial loss was applied to make SR images highly similar to real HR images using generative adversarial network (GAN) [33] in [18, 20, 23, 24, 26, 31].

The content loss has the same limitations as the use of MSE in the pixel space. It measures difference at each position equally on the whole feature map, which also causes average of possible solutions. To address this problem, we construct salient content loss function to highlight the feature-rich regions according to multi-channel response of images. The salient content loss makes the perceptual quality of regions absorbing eye focus higher than other regions by weighting feature maps. Inspired by [29], we attach morphological component discriminator and color discriminator to constrain color consistency and morphological component (e.g. texture and structure) recovery for generating natural and real SR images. Owe to those improvements, minimizing the perceptual loss composed of salient content loss, color adversarial loss, and morphological component adversarial loss favors image visual quality.

Our main contributions are:

1. We propose salient content loss function which focuses on feature-rich image content via weighting feature maps instead of the MSE-based feature loss function.
2. The color adversarial loss and the morphological component adversarial loss are applied to recover the finer color and morphological component of images.
3. Experimental results show that the proposed method achieve significant improvements on perceptual index.

This paper is organized as follows. Section 2 reviews the related work briefly. We describe the network architecture and elaborates on the perceptual loss function in Section 3. The experimental results of the SR and their evaluation are shown in Section 4. Finally, we conclude our work in Section 5.

## 2 Related work

To date CNN-based methods have made progress for SR. Since Dong et al. [9] introduced CNN into super-resolution, researchers [10, 13, 14, 15, 17] made various improvements based on SRCNN by modified the network framework.

For distortion-driven SR methods, Kim et al. [13] increased network depth and exploited more contextual information over images. Shi et al. [15] proposed sub-pixel convolution layer which models complex upscaling operation to improve SR image quality. Haris et al. [27] exploited iterative up- and down-sampling layers to learn different types of image degradation and high-resolution. Zhang et al. [12] applied residual channel attention network to learn high-frequency information.

For perceptual-quality driven SR methods, loss function is central to SR model optimization. The common loss function is pixel-based loss, which measures MSE and absolute error. It is widely used in distortion-driven SR methods due to the high correlation with PSNR. Perceptual-quality driven SR methods [18, 23, 24, 26] also applied pixel loss to pre-train SR model for preventing the SR model from local optimization. Moreover, Johnson et al [21] proposed the content loss which measures the difference

between the feature maps for ensuring feature representation of SR images to match feature of HR images. Low-level and high-level feature maps are extracted from generated HR images  $I_{SR}$  and ground truth HR images  $I_{HR}$  through the shallow layer and deeper layer of pre-trained network, respectively. Some [19, 21, 24, 26] used low-level feature maps from shallow layers of pre-trained model, others [18, 23] used higher-level feature maps from deeper layers, while others [20] used a combination of the shallow and deeper layers. Sajjadi et al. [20, 21] employed texture loss [22] which forces consistent image style using Gram matrix for realistic texture details recovery. Adversarial loss was applied to learn the statistics of natural images and greatly improved the visual quality in [18,19,20,26,31]. Park et al. [23] applied not only image-based adversarial loss but also feature-based adversarial loss to produce visually satisfactory results. Roey et al. [26] proposed the contextual loss to generate images with natural feature distributions for avoiding artifacts of SR images. Cheon et al. [31] proposed the perceptual image content loss by applying the DCT and differential operation on images for the trade-off between perception and distortion. A combination of multiple loss functions [20,24,25,31] has widely been used for visual quality enhancement. These improvements are for all features of the image, but it is not known which features contribute to image visual quality enhancement.

In this study, we aim at recovering morphological component and color details exactly by incorporate both two novel adversarial loss functions and salient content loss function to produce visually realistic SR images.

### 3 method

We employ the recently developed SRGAN model [18] as the benchmark model. The generative network  $G$  also has 16 residual blocks like [18] but removes all BN layers, as shown in Fig.1. Given an LR image  $I_{LR}$ , the goal of super-resolution task is to estimate the generated high-resolution image  $I_{SR} = G(I_{LR})$ .  $I_{LR}$  is the low-resolution version of its target high-resolution image  $I_{HR}$ . The target images are only used for training network.

Multiple theories point that the visual system applies neuronal filters on image to decompose the stimulus into features and regions of different spatial frequencies, colors, and orientations [34,35]. We employ the morphological component and color discriminator to lessen differences on texture, orientations, and color between SR images and HR images. Furthermore, it is found that visual attention is drawn to salient regions which are the aggregation of multiple features. The salient content loss is proposed based on visual attention. And our loss function  $\mathcal{L}$  is composed of the pixel loss  $\mathcal{L}_{pixel}$ , adversarial loss  $\mathcal{L}_{adv}$  and salient content loss  $\mathcal{L}_{sc}$ , as shown in Fig.2. The details of the loss functions are described below.

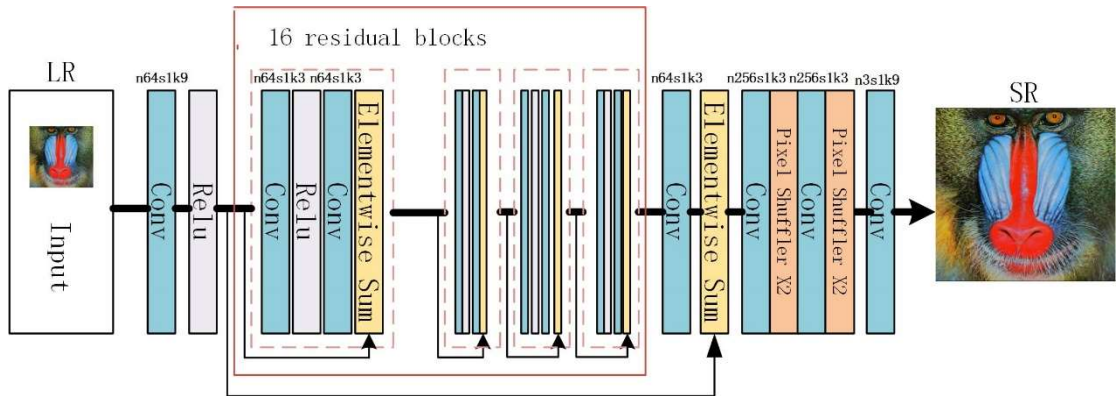


Fig.1 The network architecture of SR model.

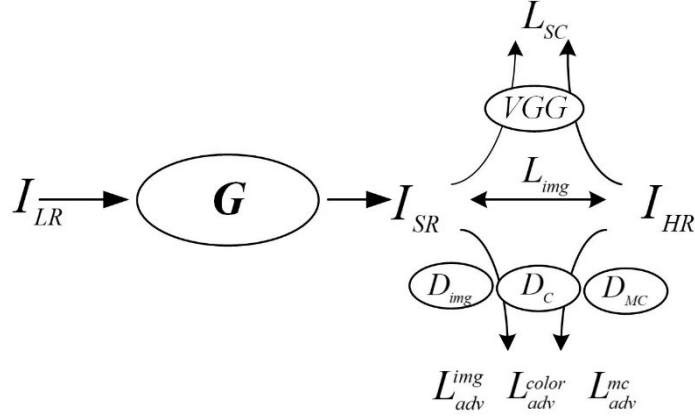


Fig. 2 The proposed visual perceptual loss function.

### 3.1 Pixel loss function

We measure pixel-wise difference between the generated HR image  $I_{SR}$  and the target image  $I_{HR}$  based on MSE, and pixel loss  $\mathcal{L}_{pixel}$  is defined as followed:

$$\mathcal{L}_{pixel} = \frac{1}{hwc} \sum (I_{SR} - I_{HR})^2 (1)$$

where  $h$ ,  $w$  and  $c$  are the height, width and number of channels of the images to be measured, respectively. It constrains  $I_{SR}$  to be close enough to  $I_{HR}$  on the pixel values.

### 3.2 Adversarial loss function

Discriminator forces the data distribution of SR images consistent with that of real HR images by distinguishing  $I_{SR}$  from  $I_{HR}$  in [18,20,24,26,28,31]. It greatly improves the visual quality of SR images, but there are many unnatural features in the reconstructions. Note that the color, texture, and structure regardless of the type or content of image are perceived exclusively through vision. We apply image discriminator  $D_{img}$  to learn statistics of natural images and attach color discriminator  $D_c$  and morphological components discriminator  $D_{MC}$  to learn color and morphological component distribution of real HR images. The color adversarial loss and morphological component adversarial loss are beneficial to visual quality enhancement based on human visual perception. The architecture of our discriminator network is shown in Fig. 3.

#### 3.2.1 color adversarial loss

The color discriminator  $D_c$  is built to reduce the color difference between SR images and ground truth HR images. The visual system captures the main color blocks of natural images including the surface color or background color of the objects while ignoring minor color details. A gaussian blur kernel  $G$  formulated as a convolutional layer is applied to reserve brightness, contrast and major color of the evaluated images while eliminating structure and texture component. The blurred images  $I_{SR}^G$  and  $I_{HR}^G$  are obtained via blurred convolution:

$$I^G = I * G \quad (2)$$

where  $I$  is the evaluated image,  $I^G$  is the blurred image,  $G$  is the blur filter, and  $*$  denotes the convolution operation. The size of filter is  $21 \times 21$ , the stride is 1, and the weights of filter are easily calculated as follow:

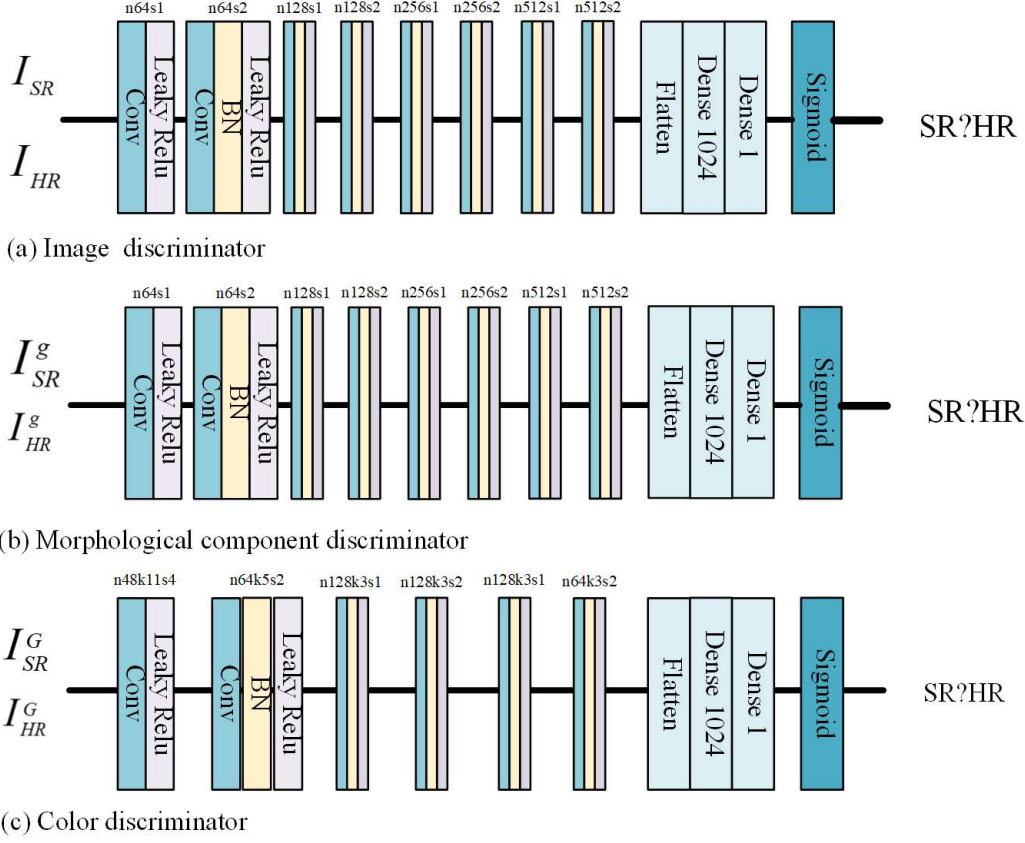


Fig. 3 (a) Architecture of image discriminator. (b) Architecture of morphological component discriminator. (c) Architecture of color discriminator. Let  $n$ ,  $k$ , and  $s$  denote the number of filters, the size of filters, and the stride, respectively. Note that the size of filters in (a) and (b) not mentioned is 3.

$$G(x, y) = \frac{1}{2\pi\sigma^2} \exp\left(-\frac{(x-\mu_x)^2}{2\sigma_x^2} - \frac{(y-\mu_y)^2}{2\sigma_y^2}\right) \quad (3)$$

where  $\mu_{x,y}$  and  $\sigma_{x,y}$  are the mean and variance of  $x$  and  $y$ , respectively. We set  $\mu_{x,y} = 0$  and  $\sigma_{x,y} = 3$ . The color discriminator ensures that the main color distribution of SR images is similar to the target HR images. The color adversarial loss measures the color difference on the blurred image, defined based on the probabilities of the discriminator  $D_c(I_{SR}^G)$  as follow:

$$\mathcal{L}_{color} = -\sum \log D_c(I_{SR}^G) \quad (4)$$

Minimizing color adversarial loss reduces color distortion and favors real and natural image generation.

### 3.2.2 Morphological component adversarial loss

The morphological components of image such as texture and structure are critical in visual perception, which are related to the image gray-level distribution and irrelevant to color or brightness. The lack of texture and structure lead to a blurred image (e.g. distortion-based SR methods) or an artificial image [32]. We apply morphological components discriminator  $D_{mc}$  to distinguish real or fake images by exploring and utilizing the difference on texture and structure between SR images and HR images. The morphological component adversarial loss  $\mathcal{L}_{mc}$  measures the difference on grayscale images which preserve all the morphological components of the image without any color component, defined as follow:

$$\mathcal{L}_{mc} = -\sum \log D_{mc}(I_{SR}^g) \quad (5)$$

where  $I_{SR}^g$  and  $I_{HR}^g$  denote grayscale SR image and grayscale HR image. Minimizing  $\mathcal{L}_{mc}$  forces SR images to have similar gray-level distributions as the target HR images and accurately recover image

morphological components.

### 3.3 Salient content loss function

The study [19,20,21] have proved the introduction of content loss improves the visual quality of generated SR images. It measures the difference equally on each spatial locations of the feature map per channel. The proposed salient content loss pays more attention the feature-rich regions which feature responses across multiple channels by spatial weighting feature maps. Minimize the difference on the weighted low-level feature maps accurately improves perceptual quality of salient regions in SR images. The high-level feature maps are also applied to constrain the feature representation of the whole image, especially the regions insensitive to human visual system. The salient content loss function  $\mathcal{L}_{SC}$  is formulated as follow:

$$\mathcal{L}_{SC} = \mathcal{L}_{low-level} + 10^{-5} \cdot \mathcal{L}_{high-level} \quad (6)$$

$$\mathcal{L}_{low-level} = \frac{1}{WHC} \sum \left( \alpha_{i,j}^{SR} \phi_{2,2}(I^{SR}) - \alpha_{i,j}^{HR} \phi_{2,2}(I^{HR}) \right)^2 \quad (7)$$

$$\mathcal{L}_{high-level} = \frac{1}{WHC} \sum \left( \phi_{5,4}(I^{SR}) - \phi_{5,4}(I^{HR}) \right)^2 \quad (8)$$

where  $W$ ,  $H$  and  $C$  are the width, height and channel of the feature maps, respectively,  $i$  and  $j$  denote the horizontal and vertical feature maps indexes, respectively.  $\phi(\cdot)$  denotes the feature maps extracted through pre-trained VGG-19 network and  $\alpha_{i,j}$  denotes the spatial weight, which is applied to each channel at that location of feature maps  $\phi_{2,2}(\cdot)^1$ . The calculation of  $\alpha_{i,j}$  is summarized in algorithm 1. Fig. 4 shows that saliency regions are highlighted by visualizing spatial weighted feature maps. The salient content loss encourages the salient regions of generated images to be perceptually similar to that of the target HR images.

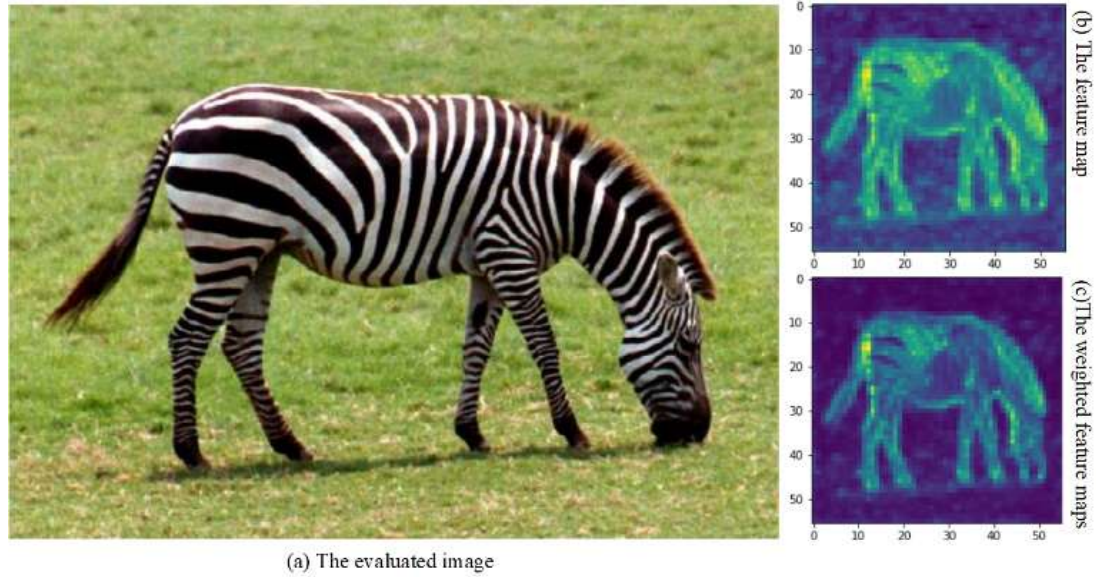


Fig.4 (a) The evaluated image (Zebra from Set14). (b) The feature map is got by fusing the feature maps ( $56 \times 56 \times 128$ ) extracted from  $\phi_{2,2}$  according to 1:1. (c) The weighted feature map is got by fusing the weighted feature maps in the same way. It is shown that the features at locations with salient visual content are boosted and feature at locations with non-salient content are down.

1.  $\phi_{2,2}$  and  $\phi_{5,4}$  are the feature maps obtained by the 2-th convolution after activation before the 2-th maxpooling layer and the 4-th convolution after activation before the 5-th maxpooling layer within the VGG19 network, respectively.

---

Algorithm 1: the calculation of spatial weight  $\alpha_{i,j}$ .

---

**Input:** Low-level feature maps  $\chi_{kij}$ . Let  $\chi_{kij} \in \mathbb{R}^{C \times W \times H}$  denote the 3-dimensional low-level feature maps from a selected layer  $\phi_{2,2}$ . Let  $i$ ,  $j$ , and  $k$  denote horizontal, vertical and channel of feature maps indexes, respectively.

1. Obtain the accumulated feature responses  $f_{i,j}^C \in \mathbb{R}^{W \times H} (i = 1, \dots, W, j = 1, \dots, H)$  by summing the feature maps  $\chi_{kij}$  per channel for each location.  $f_{i,j}^C = \sum_{k=1}^C \chi_{k,i,j}$
2. Normalize accumulated feature maps by  $L2$  norm to calculate spatial weight  $\alpha_{i,j}$ .

$$\alpha_{i,j} = \frac{f_{i,j}^C}{\sqrt{\left(\sum_{i=1}^H \sum_{j=1}^W (f_{i,j}^C)^2\right)}}$$

3. Obtain the weighted feature maps  $\hat{\chi}_{k,i,j}$ .  $\hat{\chi}_{k,i,j} = \chi_{k,i,j} \cdot \alpha_{i,j}$

**Output:** Spatial weight  $\alpha_{i,j}$ .

---

### 3.4 Total loss function

Our visual perceptual loss function is a weighted sum of above losses, defined as follow:

$$\mathcal{L} = \mathcal{L}_{pixel} + 2 \times 10^{-4} \mathcal{L}_{SC} + 10^{-3} \times \mathcal{L}_{adv}^{img} + 4 \times 10^{-6} \mathcal{L}_{adv}^{color} + 1 \times 10^{-4} \mathcal{L}_{adv}^{mc} \quad (9)$$

## 4 Experiments

### 4.1 Experiment settings

During training, we train our SR model with a scale factor of  $\times 4$  and three discriminators on NVIDIA GeForce GTX 1080ti using 800 images from DIV2K dataset. The HR images are degenerated into the LR images via downsampling using bicubic function in MATLAB. We crop 16 random  $96 \times 96$  sub-images from 800 images for each mini-batch. The Adam optimization with  $\beta_1 = 0.9$  is applied. The SR network is pre-trained with learning rate of  $10^{-4}$  and  $5 \times 10^4$  update iterations using MSE-based loss function for initialization of generator. We alternately update the generator and discriminators with learning rate of  $10^{-4}$ . After  $10^5$  update iterations, learning rate is reduced by 10 times.

During testing, we perform experiments on three benchmark datasets Set5, Set14, and BSD100, which have five, fourteen, and one hundred natural images, respectively.

### 4.2 Experiment evaluation

We compare the proposed method with the bicubic interpolation method and several state-of-the-art SR methods, including the DRCN[10], the VDSR[13], the EDSR[17], the SRGAN-MSE[18], the SRGAN-VGG22[18], the SRGAN[18], the EnhanceNet[20], the ESRGAN[24], the 4PP-EUSR[30], and the GAN-PCL[31]. The SR images of compared methods [10,13,17,18,20,24] are from their website and the objective evaluation value of compared methods [30,31] are from their paper. We use perceptual index (PI) proposed in the PIRM Challenge on perceptual super-resolution [32] to evaluate the perceptual quality of SR images instead of PSNR. The perceptual index combines the no-reference image quality measures of Ma et al. [36] and NIQE [37] as follow:

$$Pi = \frac{1}{2} \left( (10 - Ma(SR)) + NIQE(SR) \right) \quad (10)$$





Fig. 5. The SR result on the '101085' image from BSD100 at the upscaling factor of 4.

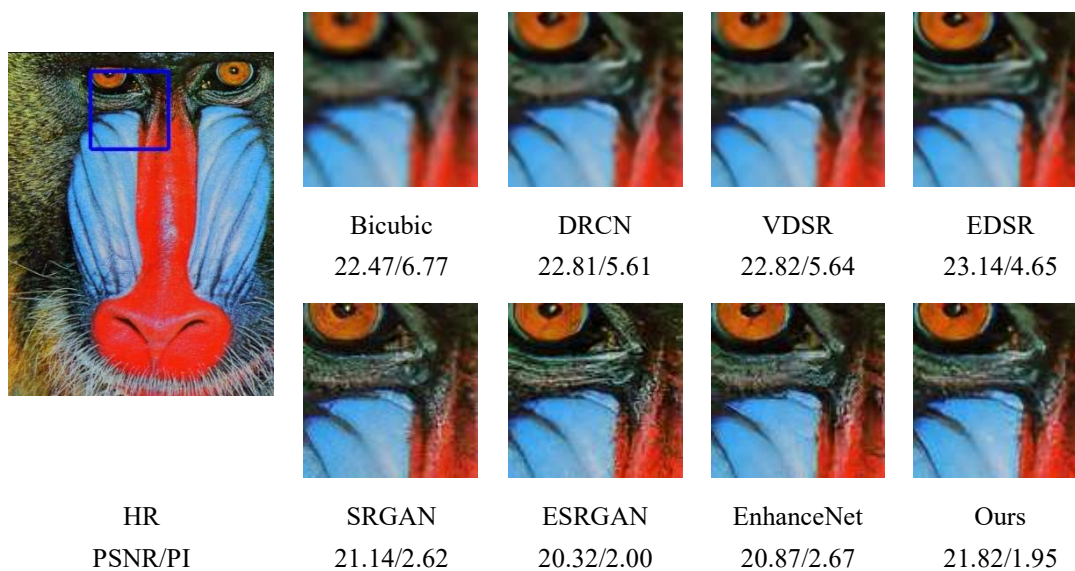


Fig. 6. The SR result on the Baboon image from Set14 at the upscaling factor of 4.

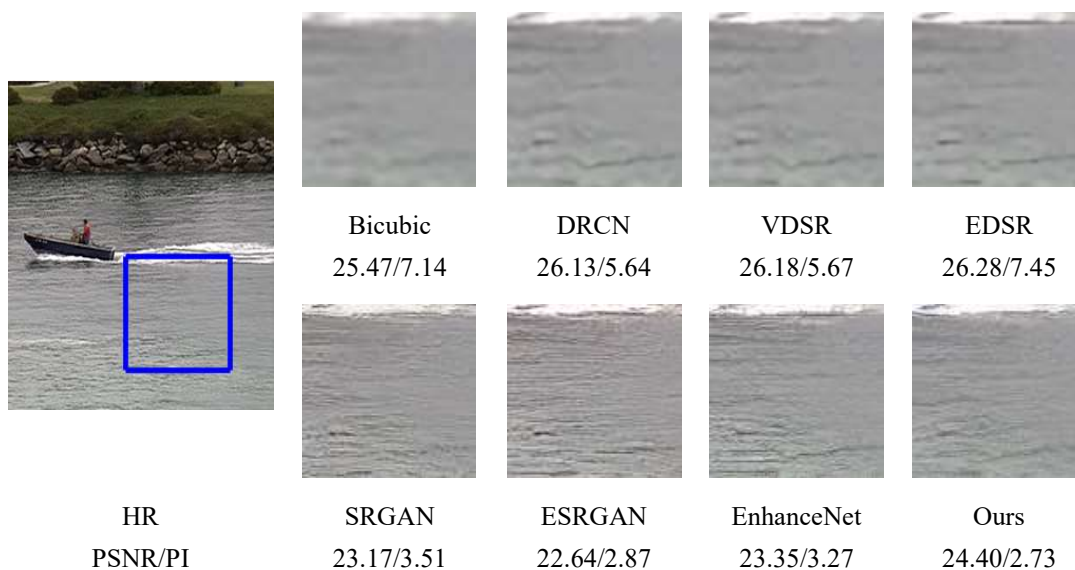




Fig. 7. The SR result on the Coastguard image from Set14 at the upscaling factor of 4.

The lower PI value and NIQE value denote the better perceptual quality. For fairly comparison, we drop four pixels of border and then measure PSNR on the luminance channel.

**Visual quality.** The results of state-of-the-art methods with ours at 4x super-resolution on visual quality are shown in Fig. 5-8. Note that perceptual-driven SR methods can recover finer high-frequency details and produce visually satisfactory results compared with the distortion-driven methods. It can be observed our SR results show the similar color and morphological components as HR images and look more natural while there are over-fake textures, less details, undesired texture in ESRGAN, SRGAN, and EnhanceNet, respectively.

Table 1. Evaluation of image quality in terms of distortion and perception.

$\times 4$	Set5			Set14			BSD100		
	PSNR	NIQM	PI	PSNR	NIQM	PI	PSNR	NIQM	PI
bicubic	28.418	8.540	7.385	26.090	7.764	7.051	25.957	7.712	6.995
DRCN	31.534	7.903	6.446	28.027	6.600	5.940	27.236	6.862	5.890
VDSR	31.349	7.812	6.297	28.015	6.467	5.696	27.287	6.677	5.700
EDSR	32.630	7.234	6.012	28.953	6.305	5.514	27.796	6.432	5.326
SRGAN-MSE	30.666	5.000	3.844	27.006	4.005	3.064	25.981	4.032	2.802
SRGAN-VGG22	29.871	4.919	3.692	26.529	4.221	3.119	25.697	3.750	2.631
SRGAN	29.410	4.651	3.355	26.114	3.875	2.882	25.176	3.407	2.397
EnhanceNet	28.564	4.264	2.926	25.770	4.130	3.018	24.930	4.525	2.908
ESRGAN	30.454	5.162	3.755	26.276	3.890	2.926	25.316	3.640	2.479
4PP-EUSR	31.085	5.607	4.229	27.622	4.172	3.200	26.570	3.698	2.744
GAN-PCL	31.568	/	4.569	28.236	/	3.552	27.113	/	3.242
Ours	28.751	4.466	3.443	25.960	3.697	2.881	24.501	3.361	2.330

**Quantitative results.** Table 1 shows the quantitative results of the proposed SR method and other SR methods. Our proposed method achieves significantly superior PI and is ranked second, first, and first for Set5, Set14, and BSD100, respectively. The average gain on PI for BSD100 achieved by our method is lower 0.14 than ESRGAN. The results verify both the validity of our method and good robustness for different kinds of input data.

## 5 Conclusion

In this paper, we propose salient content loss and transfer adversarial loss from image into the component of image including color and morphological components for improvement on the visual quality of images. Two novel loss function are combined to train SR model. The experimental results indicate the superiority of the proposed method over the other tested methods. Compared to the other most-commonly used methods, our method provides better edge structures and textures, and produce visual satisfactory result.

## 6. References

1. Yue L, Shen H, Li J, et al. Image super-resolution: The techniques, applications, and future[J].

Signal Processing, 2016: S0165168416300536.

2. Wang Z, Chen J, Hoi S C H Deep Learning for Image Super-resolution: A Survey[J]. 2019.
3. Li X, Orchard M T. New edge-directed interpolation[J]. IEEE Transactions on Image Processing, 2001, 10(10):1521-1527.
4. Dengwen Z. An edge-directed bicubic interpolation algorithm[C]// International Congress on Image & Signal Processing. IEEE, 2010.
5. Chang N H, Yeung D Y, Xiong N Y. Super-resolution through neighbor embedding[C]// Proceedings of the 2004 IEEE Computer Society Conference on Computer Vision and Pattern Recognition. IEEE Computer Society, 2004.
6. Timofte R, De V, Gool L V. Anchored Neighborhood Regression for Fast Example-Based Super-Resolution[C]// 2013 IEEE International Conference on Computer Vision (ICCV). IEEE Computer Society, 2013.
7. Yang J, Wright, Huang T S, et al. Image super-resolution via sparse representation[J]. IEEE Transactions on Image Processing, 2010, 19(11).
8. Russakovsky O, Deng J, Su H, et al. ImageNet Large Scale Visual Recognition Challenge[J]. International Journal of Computer Vision, 2014, 115(3):211-252.
9. Dong C, Loy C C, He K, et al. Learning a Deep Convolutional Network for Image Super-Resolution[J]. 2014.
10. Kim J, Lee J K, Lee K M. Deeply-Recursive Convolutional Network for Image Super-Resolution[C]// 2016 IEEE Conference on Computer Vision and Pattern Recognition (CVPR). IEEE, 2016.
11. He K, Zhang X, Ren S, et al. Deep Residual Learning for Image Recognition[J]. 2015.
12. Zhang Y, Li K, Li K, et al. Image Super-Resolution Using Very Deep Residual Channel Attention Networks[J]. 2018.
13. Kim J, Lee J K, Lee K M. Accurate Image Super-Resolution Using Very Deep Convolutional Networks[C]// 2016 IEEE Conference on Computer Vision and Pattern Recognition (CVPR). IEEE, 2016.
14. Tai Y, Yang J, Liu X. Image Super-Resolution via Deep Recursive Residual Network[C]// IEEE Computer Vision and Pattern Recognition (CVPR 2017). IEEE, 2017.
15. Shi W, Caballero J, Huszár, Ferenc, et al. Real-Time Single Image and Video Super-Resolution Using an Efficient Sub-Pixel Convolutional Neural Network[J]. 2016.
16. Tong T, Li G, Liu X, et al. Image Super-Resolution Using Dense Skip Connections[C]// 2017 IEEE International Conference on Computer Vision (ICCV). IEEE Computer Society, 2017.
17. Lim B, Son S, Kim H, et al. Enhanced Deep Residual Networks for Single Image Super-Resolution[J]. 2017.
18. Ledig C, Theis L, Huszar F, et al. Photo-Realistic Single Image Super-Resolution Using a Generative Adversarial Network[J]. 2016.
19. Dosovitskiy A, Brox T. Generating Images with Perceptual Similarity Metrics based on Deep Networks[J]. 2016.
20. Sajjadi M S M, Schölkopf, Bernhard, Hirsch M. EnhanceNet: Single Image Super-Resolution Through Automated Texture Synthesis[J]. 2016.
21. Johnson J., Alahi A., Fei-Fei L. (2016) Perceptual Losses for Real-Time Style Transfer and Super-Resolution. In: Leibe B., Matas J., Sebe N., Welling M. (eds) Computer Vision – ECCV 2016. ECCV 2016. Lecture Notes in Computer Science, vol 9906. Springer, Cham

22. Gatys L A, Ecker A S, Bethge M. Texture synthesis using convolutional neural networks[C]// International Conference on Neural Information Processing Systems. MIT Press, 2015.
23. Park S J, Son H, Cho S, et al. SRFeat: Single Image Super-Resolution with Feature Discrimination: 15th European Conference, Munich, Germany, September 8-14, 2018, Proceedings
24. ESRGAN: Enhanced super-resolution generative adversarial networks.  
<https://arxiv.org/abs/1809.00219v2>
25. Yuan Y, Liu S, Zhang J, et al. Unsupervised Image Super-Resolution using Cycle-in-Cycle Generative Adversarial Networks[J]. 2018.
26. Mechrez R, Talmi I, Shama F, et al. Maintaining Natural Image Statistics with the Contextual Loss[J]. 2018.
27. Haris M, Shakhnarovich G, Ukita N. Deep Back-Projection Networks For Super-Resolution[J]. 2018.
28. Yang C Y, Ma C, Yang M H. Single-Image Super-Resolution: A Benchmark[J]. 2014.
29. Ignatov A, Kobyshev N, Timofte R, et al. DSLR-Quality Photos on Mobile Devices with Deep Convolutional Networks[C]// 2017 IEEE International Conference on Computer Vision (ICCV). IEEE Computer Society, 2017.
30. Choi J H, Kim J H, Cheon M, et al. Deep Learning-based Image Super-Resolution Considering Quantitative and Perceptual Quality[J]. 2018.
31. Cheon M, Kim J H, Choi J H, et al. Generative adversarial network-based image super-resolution using perceptual content losses[J]. 2018.
32. Blau Y, Mechrez R, Timofte R, et al. 2018 PIRM Challenge on Perceptual Image Super-resolution[J]. 2018.
33. Goodfellow I J, Pouget-Abadie J, Mirza M, et al. Generative Adversarial Nets[C]// International Conference on Neural Information Processing Systems. MIT Press, 2014.
34. Christoph Rößing. Human Visual Perception[M]// Handbook of Camera Monitor Systems. Springer International Publishing, 2016.
35. Landy, M.S., Graham, N.: Visual perception of texture. In: Chalupa, L.M., Werner, J.S. (eds.) The Visual Neurosciences, pp. 1106–1118. MIT Press, Cambridge (2004). ch. 9
36. Ma C, Yang C Y, Yang X, et al. Learning a no-reference quality metric for single-image super-resolution[J]. Computer Vision and Image Understanding, 2017, 158:1-16.
37. Mittal A, Follmann, IEEE, et al. Making a 'Completely Blind' Image Quality Analyzer[J]. IEEE Signal Processing Letters, 2013, 20(3):209-212.